Published in final edited form as:
Biomaterials. 2008 ; 29(24-25): 3415–3428. doi:10.1016/j.biomaterials.2008.05.002.

In vivo Degradation of Three-Dimensional Silk Fibroin Scaffolds

Yongzhong Wang[1], **Darya D. Rudym**[1], **Ashley Walsh**[2], **Lauren Abrahamsen**[2], **Hyeon-Joo Kim**[1], **Hyun Suk Kim**[3], **Carl Kirker-Head**[1,2], and **David L. Kaplan**[1,*]

[1]Departments of Chemical and Biological Engineering, Chemistry & Biomedical Engineering, Tufts University, 4 Colby Street, Medford, MA 02155

[2]Department of Clinical Sciences, Cummings School of Veterinary Medicine, Tufts University, 200 Westboro Road, North Grafton, Massachusetts 01536

[3]Department of Polymer Science and Engineering, Inha University, Incheon 402-751, Korea

Abstract

Three-dimensional porous scaffolds prepared from regenerated silk fibroin using either an all aqueous process or a process involving an organic solvent, hexafluoroisopropanol (HFIP) have shown promise in cell culture and tissue engineering applications. However, their biocompatibility and *in vivo* degradation has not been fully established. The present study was conducted to systematically investigate how processing method (aqueous vs. organic solvent) and processing variables (silk fibroin concentration and pore size) affect the short-term (up to 2 months) and long-term (up to 1 year) *in vivo* behavior of the protein scaffolds in both nude and Lewis rats. The samples were analyzed by histology for scaffold morphological changes and tissue ingrowth, and by real-time RT-PCR and immunohistochemistry for immune responses. Throughout the period of implantation, all scaffolds were well-tolerated by the host animals and immune responses to the implants were mild. Most scaffolds prepared from the all aqueous process degraded to completion between two and six months, while those prepared from organic solvent (hexafluoroisopropanol (HFIP)) process persisted beyond one year. Due to widespread cellular invasion throughout the scaffold, the degradation of aqueous-derived scaffolds appears to be more homogeneous than that of HFIP-derived scaffolds. In general and especially for the HFIP-derived scaffolds, a higher original silk fibroin concentration (e.g. 17%) and smaller pore size (e.g. 100–200 μm) resulted in lower levels of tissue ingrowth and slower degradation. These results demonstrate that the *in vivo* behavior of the three-dimensional silk fibroin scaffolds is related to the morphological and structural features that resulted from different scaffold preparation processes. The insights gained in this study can serve as a guide for processing scenarios to match desired morphological and structural features and degradation time with tissue-specific applications.

1. Introduction

Silks are naturally occurring fibrous proteins commonly produced by insects and spiders. They exhibit a unique and useful combination of properties such as being degradable and light weight with excellent mechanical and thermal properties [1–3]. In nature silks are used

*Correspondence: David L. Kaplan, Departments of Biomedical Engineering & Chemical and Biological Engineering, Tufts University, Science and Technology Center, 4 Colby Street, Medford, MA 02155, USA. Tel: 617-627-3251, Fax: 617-627-3231, david.kaplan@tufts.edu.

as materials for web construction and prey capture (spider webs), safety line (draglines) and reproduction enclosures (cocoons) [1, 2, 4–9]. These features also relate to the use of native silks as sutures, although they are being gradually replaced by synthetic polymers [6, 10–14]. Beyond their traditional use as sutures, silk fibroin has been exploited as a biomaterial for cell culture and tissue engineering *in vitro* and *in vivo* since mid-1990's [15]. In early studies, silk films prepared from native silkworm fibroin collected from glands of *Bombyx mori* domestic silkworms and *Antheraea pernyi* wild silkworms were found to support the attachment and proliferation of murine fibroblasts [16, 17]. Later reports showed that regenerated silk films prepared by dissolving silkworm cocoon fibers in 9–9.5 M LiBr supported the attachment and growth of human and animal cell lines [18, 19]. These studies provided early clues to the utility of regenerated silk fibroin as a scaffold/matrix biomaterial for cell culture and tissue engineering. Over the past decade, numerous studies have explored regenerated silk fibroin-based biomaterials in various forms, including films, membranes, mats, nets, hydrogels, and porous sponges for biomedical applications [15].

The *in vivo* behavior of biomaterials prepared from regenerated silk fibroin solutions has not been fully demonstrated, despite the fact that the biocompatibility and degradation of silk sutures, which are prepared from native silk fibers, has been well established [6, 15]. Previous studies showed that two-dimensional silk fibroin films have good biocompatibility [6, 20–22]. Recent progress in processing techniques has yielded three-dimensional porous silk fibroin scaffolds with control of morphological and structural features [23–25]. The three-dimensional porous scaffolds have been prepared using either an all aqueous process or a process involving organic solvent, hexafluoroisopropanol (HFIP) [23–25]. The promise of the 3-dimensional scaffolds by themselves, or in combination with cells, for biomedical applications has been demonstrated extensively *in vitro* and *in vivo* [15, 22, 26–42]. However, the *in vivo* degradation of these three-dimensional silk fibroin scaffolds has not been systematically investigated.

The goal of the present study was to systematically examine the relationship between the morphological and structural features of the silk fibroin three-dimensional scaffolds and their biological reactions *in vivo*. Specifically, we were interested in assessing the effect of scaffold processing variables (e.g., water vs. organic solvent), silk concentration, and pore size on the short-term and long-term *in vivo* behavior. The study consisted of two stages. Stage I was a short term (8 week) intramuscular implantation in nude and Lewis rats designed to quickly obtain initial information on the role of immune system on the degradation of the scaffolds derived from aqueous or HFIP processes. Based on the information obtained from Stage I, a long term (1 year) Stage II study was carried out using scaffolds prepared from aqueous and HFIP processes with varying silk fibroin concentrations and pore sizes and implanted subcutaneously in Lewis rats.. The samples were analyzed by histology for morphological changes, and real-time RT-PCR and immunohistochemistry for immune responses.

2. Materials and Methods

2.1 Preparation of three-dimensional silk fibroin scaffolds

Three-dimensional silk fibroin scaffolds were prepared from *Bombyx mori* silkworm cocoons according to the procedures described in our previous studies [23–25, 41], as summarized in a previous review [15]. Briefly, the cocoons were extracted in a 0.02M Na_2CO_3 solution, dissolved in a 9.3M LiBr solution and subsequently dialyzed against distilled water to obtain silk fibroin aqueous solutions at varying concentrations. To form the aqueous-derived scaffolds, four grams of granular NaCl particles in varying size ranges (106–212 μm, 500–600 μm, and 850–1000 μm) were directly added to 2 ml of a silk fibroin aqueous solutions (6% and 10%) in Teflon cylinder containers and remained at room

temperature for 24 hours. Then the containers were immersed in water to extract the salt from the porous scaffolds for two days. To form the HFIP-derived scaffolds, the silk fibroin aqueous solution was freeze-dried and then dissolved in HFIP (6% and 17%). Granular NaCl particles in various size ranges (106–212 μm, 500–600 μm, and 850–1000 μm) were then added and lyzed against water to obtain the scaffolds. Generally the pore size of the resultant scaffolds was slightly smaller than the original size of the granular NaCl particles, as evaluated by a LEO Gemini 982 field emission gun scanning electron microscopy (SEM) [24]. For example, the pore size of scaffolds prepared using 500 to 600 μm NaCl particles was 550±30 μm. In the following context, the scaffolds were grouped approximately by the original size ranges of the NaCl particles (100–200 μm, 500–600 μm, and 850–1000 μm). For *in vivo* evaluation, the scaffolds were cut into discs (5 mm in diameter and 2.5 mm in thickness), dried in a fume hood, autoclaved, and kept in PBS before implantation.

2.2 Implantation of three-dimensional silk fibroin scaffolds

The evaluation of the three-dimensional silk fibroin scaffolds was carried out in two stages (Table 1). The first stage of the study was a short (8 week) implantation aiming to obtain initial information on the degradation of silk fibroin scaffolds prepared by the two different processes, aqueous- and HFIP-derived silk scaffolds prepared with 6% silk fibroin solution with the same pore size (500 to 600 μm). These samples were implanted in muscle pouches of athymic T-cell deficient RH-rnu and Lewis rats randomly (Stage I in Table 1). The animals were sacrificed to retrieve the scaffolds for analysis 8 weeks after implantation. Based on the information obtained from this first stage of study, aqueous-derived and HFIP-derived silk scaffolds with varying concentrations of silk fibroin and pore sizes were subcutaneously implanted in Lewis rats (Stage II in Table 1). The combinations of concentrations and pore sizes used in this study were selected based on previous studies [23] and covered the processing windows of these two types of scaffolds.

All *in vivo* procedures were approved by the Tufts Cummings School of Veterinary Medicine Institutional Animal Care and Use Committee. Buprenorphine (0.05mg/kg SQ) and procaine penicillin (200,000IU/kg IM) were administered pre-surgically. In every case, the rats weighing approximately 350 g were then maintained under general anesthesia using inhalant isofluorane and oxygen. Animals were first positioned in dorsal recumbency and the ventral abdomen was aseptically prepared for surgery. Four approximately 5 mm long skin incisions were created (2 cranially and abaxial to the mid-line axis; 2 caudally and abaxial to the mid-line axis) and the underlying subcutaneous tissue +/− muscle bellies were divided to provide tissue beds for the implants. Following implantation, muscle bellies were closed with size 3-0 absorbable suture. Skin was closed with metallic wound clips. Rats were then repositioned in ventral recumbency, their backs were aseptically prepared for surgery, and four additional implant sites were similarly created abaxial to the vertebral column (2 cranial and 2 caudal). Carprofen (5mg/kg SQ) was administered as an analgesic once daily for at least 48 hours post-surgery. Wound clips were removed under short acting isoflurane inhalant anesthesia 7 days post-surgery. A total of 432 scaffolds were implanted in a total of 56 rats with 8 scaffolds per rat for 48 rats and 6 scaffolds per rat for the other 8 rats (Stage II in Table 1). All animals used in this study were male. The scaffolds were implanted randomly in the animals.

Due to process limitations, aqueous-derived scaffolds with original silk fibroin solution at concentrations higher than 10% were not obtainable, making it impractical to compare them with HFIP-derived scaffolds at the same original silk fibroin solutions at the high end (e.g. 17 wt %) of the concentration range. The animals were sacrificed to retrieve the scaffolds at 2 weeks, 2 months, 6 months, and 1 year after implantation for analysis. No signs of abnormality were observed during the gross examination of the animals and implants at the time of the sacrifices.

2.3 Sample Treatment and Total RNA Extraction, cDNA Synthesis, and Real-time RT-PCR Analysis

Total RNA was extracted from tissue samples containing the scaffolds using an RNeasy Mini Kit (Qiagen, Valencia, CA, USA) following the supplier's instructions. Subcutaneous tissue away from the implantation site was used as control. Briefly, the explanted samples were trimmed of excessive peripheral tissue, cut into small pieces, homogenized in supplied lysis buffer, and run through a QIAshredder spin column. Ethanol was added to the homogenized lysate before the samples were purified by a RNeasy spin column. For PCR, cDNA was synthesized from the total RNA using a High-Capacity cDNA Archive kit (Applied Biosystems, Foster City, CA, USA) following the supplier's instructions. The real-time RT-PCR reactions were conducted and monitored with an ABI Prism 7000 Sequence Detection System (Applied Biosystems). TaqMan® Gene Expression assay kits (Applied Biosystems) were used for transcript levels of tumor necrosis factor alpha (TNF-α, reference sequence NM_012675.2), interleukin-4 (IL-4, reference sequence NM_201270.1), interleukin-6 (IL-6, reference sequence NM_012589.1), interleukin 13 (IL-13, reference sequence NM_053828.1), and interferon-gamma (IFN-γ, reference sequence NM_138880.2). A 50 μl reaction with 5 μl of cDNA from each sample was mixed with 2.5 μl of the assays-on-demand kit, 17.5 μl of RNase/DNase free water, and 25 μl of 2x TaqMan® Universal PCR Master Mix (Applied Biosystems). Final data were analyzed by ABI Prism 7000 Sequence Detection Systems version 1.0 software supplied by the vendor (Applied Biosystems). The Ct value for each sample was defined as the cycle number at which the fluorescence intensity reached a certain threshold where amplification of each target gene was within the linear region of the reaction amplification curves. Relative expression level for each target gene was normalized by the Ct value of TaqMan® Rodent housekeeping gene GAPDH using an identical procedure ($2^{\Delta Ct}$ formula, Perkin Elmer User Bulletin #2). When analyzing the data, undetected levels were treated as 0. Each sample was analyzed in triplicate.

2.4 Histology and immunohistochemistry

The samples harvested at different time points were washed in PBS, and fixed in 10% neutral buffered formalin before histological and immunohistochemical analysis. Samples were dehydrated through a series of graded alcohols, embedded in paraffin and sectioned at 5 μm thickness. For histological evaluation, sections were deparaffinized, rehydrated through a series of graded alcohols, and stained with hematoxylin and eosin (H&E). For immunohistochemical evaluation of macrophage invasion, sections were incubated with a monoclonal antibody against rat macrophages and giant cells (ED1, Serotec, Raleigh, NC, USA) and a horseradish peroxidase (HRP)-labeled secondary antibody. The samples were processed with a BenchMark automated histology staining system (Ventana, Tucson, AZ, USA). Sections were counterstained with hematoxylin. All sections were evaluated with a Zeiss Axiovert S100 light microscope and a Sony Exwave HAD 3CCD color video camera. The intramuscular pouch used during the first stage of the study was a more confined space than the subcutaneous site used during the second stage of the study. Therefore, sections of scaffolds implanted intramuscularly during the first stage of the study were used to estimate the relative size of the remaining scaffolds based on the area occupied by scaffolds in these sections using the Scion Image software.

2.5 Statistical analysis

All assays were repeated with a minimum of N=3. Data were analyzed with statistically significant values defined as $p<0.05$ based on one-way analysis of variance (ANOVA).

3. Results

3.1 Intramuscular degradation of three dimensional silk fibroin scaffolds in nude and Lewis rats

3.1.1 Morphology—During the first stage of the study, aqueous-derived and HFIP-derived silk scaffolds in the same pore size range (500 to 600 μm) were implanted in muscle pouches of nude and Lewis rats and harvested 8 weeks later. The purpose of this short experiment was to obtain preliminary insight into the effects of different processes on immune system responses related to the degradation of the three-dimensional silk fibroin scaffolds. During the 8 weeks, the scaffolds were tolerated well by the host animals and no abnormal conditions were observed based on gross analysis as well as histologically.

Scaffolds prepared by the two different processes showed clear differences in degradation characteristics *in vivo*. Heavy tissue ingrowth occurred at the implantation site of the aqueous-derived scaffolds. At 8 weeks, these scaffolds were completely infiltrated and largely lost their structural integrity with most pores having collapsed (Fig. 1 A, B, E, and F). As a result, the scaffolds shrank in total size when this pore structure was lost, when compared to the original size prior to implantation (Fig. 1 I). This is more evident in Lewis rats than in nude rats. After 8 weeks *in vivo*, the cross sectional area of the water-derived scaffolds in Lewis rats was about 1/3 of that in nude rats (Fig. 1 K). In contrast, although tissue ingrowth was also significant in the HFIP-derived scaffolds at 8 weeks, the scaffolds were not completely infiltrated (Fig. 1 C, D, G, and H). There were still unfilled cavities, especially in the center of the HFIP-derived scaffolds. Although tissue ingrowth changed the size and orientation of some pores in the HFIP-derived scaffolds, the scaffolds were for the most part still structurally intact in both Lewis and Nude rats at 8 weeks.

3.1.2 Immune response—The immune system played a significant role in the degradation rate of the aqueous-derived scaffolds but did not show the same impact on the HFIP-derived scaffolds. There was no significant difference between nude and Lewis rats in the cross sectional area of the HFIP-derived scaffolds at the end of 8 weeks (Fig. 1 K). Overall, the size of the aqueous-derived scaffolds was smaller than that of the HFIP-derived scaffolds. The most significant difference between the two types of scaffolds appeared in Lewis rats, where the cross sectional area of the aqueous-derived scaffolds was about 20% of that of HFIP-derived scaffolds (Fig. 1 K). This difference reflects the dramatic difference in the structural integrity of the two types of scaffolds (water vs. organic solvent processed) and tissue ingrowth after 8 weeks *in vivo* (Fig. 1 A–H).

In Lewis rats, macrophages were present at the implantation sites of the HFIP-derived scaffolds (Fig. 2 A) and aqueous-derived scaffolds (Fig. 2 B). Most macrophages detected at the implantation sites of HFIP-derived scaffolds appeared in clusters (Fig. 2 A). Aqueous-derived scaffolds appeared to be less resistant to macrophage degradation than the HFIP-derived scaffolds (Fig. 2).

3.2 Subcutaneous degradation of three dimensional silk fibroin scaffolds in Lewis rats

3.2.1 Morphologies of scaffolds after short term implantation (up to 8 weeks)—Based on the results of Stage I, Lewis rats were selected as the host for Stage II, a 1 year investigation. The aqueous-derived scaffolds were quickly infiltrated upon implantation. After two weeks *in vivo*, all aqueous-derived scaffolds prepared from 6% silk fibroin solutions began to lose their structural integrity and were almost completely filled by invading cells (Fig. 3 A and B). In contrast, aqueous-derived scaffolds prepared from a more concentrated (10%) silk fibroin solution largely held their structural integrity (Fig. 3 C and D). Despite significant tissue ingrowth, there were still unfilled pores in the aqueous-derived

scaffolds prepared from 10% silk fibroin solution (Fig. 3 C and D). At the end of 8 weeks, aqueous-derived scaffolds prepared from 10% silk fibroin solution still held structural integrity to some degree and large remaining pieces of scaffold were morphologically similar to those at the end of 2 weeks (Fig. 3 G and H).

All HFIP-derived scaffolds largely held their structural integrity within 8 weeks *in vivo* (Fig. 4). Similar to the case for aqueous-derived scaffolds, HFIP-derived scaffolds prepared from more concentrated silk fibroin solutions had less initial tissue ingrowth as evidenced by more unfilled pores especially toward the center of the scaffolds (Fig. 4). Pore size played a significant role in tissue ingrowth in the HFIP-derived scaffolds during the early stages of *in vivo* implantation. The HFIP scaffolds prepared from the most concentrated silk fibroin solution (17%) with the smallest pore size (100 to 200 μm) had the largest unfilled space at week 2 and week 8 (Fig. 4). At the end of 8 weeks, most HFIP-derived scaffolds were still not completely infiltrated, although tissue ingrowth generally progressed when compared to 2 weeks (Fig. 4).

3.2.2 Vascularization of scaffolds after short term implantation (till 8 weeks)— As part of tissue ingrowth, vascularization was observed in both types of scaffolds at 2 and 8 weeks (Fig. 5). Histological evaluations did not reveal significant difference in vascularization between the two types of scaffolds.

3.2.3 Morphologies of scaffolds after long term implantation (6 to 12 months) —At the end of 6 and 12 months, 11 out of 12 aqueous-derived scaffolds prepared from 6% silk fibroin solution completely degraded (Table 2). Only traces of the remains of one aqueous-derived scaffold with 500 to 600 μm pore size were found under a microscope at high magnification at both timepoints (Fig. 6 A and B). Residuals of aqueous-derived scaffolds prepared from a more concentrated (10%) silk fibroin solution were found in 4 out of 6 samples at 6 months and 2 out of 6 samples at 12 months (Table 2). The number and size of residuals of these scaffolds sharply diminished at the end of 12 months compared to 6 months (Fig. 6 C–F). At the end of 12 months, only very few small pieces were found throughout the implantation sites (Fig. 6 E).

The HFIP-derived scaffolds lasted significantly longer than the aqueous derived scaffolds. Remains of HFIP-derived scaffolds were found in all implantation sites at 6 and 12 months (Table 2). Similar to the short term observations, the long term impact of pore size and concentration of the original silk fibroin solution on the infiltration and structural integrity of HFIP-derived scaffolds was exemplified by scaffolds prepared from the most concentrated silk fibroin solution (17 wt%), especially those with smallest pore size (100 to 200 μm). These scaffolds (17 wt% silk, 100 to 200 μm pores) exhibited the best structural integrity and worst tissue ingrowth among all scaffolds at the end of 6 months (Fig. 7 A). Even after 1 year *in vivo*, there were still many unfilled areas visible in these scaffolds (Fig. 7 B). In contrast, most of other HFIP-derived scaffolds lost their structural integrity at 6 months (Fig. 7 C as an example). At the end of one year, most of these scaffolds were left with separate small pieces, which sometimes were not easy to find (Fig. 7 D as an example).

3.2.4 Short term Immune response (up to 8 weeks)—Within the first 8 weeks, the scaffolds were well tolerated by the host animals and no abnormal conditions were observed. Signs of granulomatomous inflammation were visible adjacent to the scaffolds based on the presence of multinucleated giant cells (Fig. 5 D) and macrophages (Fig. 8 A–F). The initial immune response to the aqueous-derived scaffolds with different pore sizes and original silk fibroin concentration was similar at 2 weeks (Fig. 8 A and B). Macrophages invaded these scaffolds and started to concentrate around the individual scaffold pieces. Signs of scaffold fragmentation were visible (Fig. 8 A and B). At the end of 8 weeks, the

signs of degradation became more evident (Fig. 8 C and D). Among aqueous-derived scaffolds, the degradation appeared to be more advanced in those prepared from lower original silk fibroin concentrations (Fig. 8 A–D).

In the HFIP-derived scaffolds, macrophages invaded but clear signs of scaffold breakdown were rare at the end of 2 weeks (Fig. 8 E). As shown earlier, these HFIP-derived scaffolds were for the most part structurally intact after 2 weeks *in vivo*. At the end of 8 weeks, most of these scaffolds still held their structural integrity; however, signs of degradation were observable, although far less prevalent compared to the aqueous-derived scaffolds (Fig. 8 F).

At the end of 2 weeks, the expression of inflammation-related mRNAs was generally very low and remained local (Fig. 9). When normalized to the house keeping gene GAPDH, the relative expression level was in the magnitude of 10^{-4} for TNF-α and IL-6 mRNAs and 10^{-6}–10^{-5} for IFN-γ mRNAs, which in some cases was not detectable (Fig. 9). The IL-4 and IL-13 mRNAs were barely detectable or not detectable at all at 2 weeks with the average relative expression level in the range of 10^{-7}–10^{-6} (Fig. 9). Given the extremely low level, comparing expression levels for IFN-γ, IL-4 and IL-13 mRNAs between different groups was not meaningful. For TNF-α and IL-6, there was no clear trend or difference observed in their relative expression levels in HFIP-derived scaffolds at 2 weeks (Fig. 9). Among aqueous-derived scaffolds, only scaffolds prepared from 10% silk fibroin solution showed expression of TNF-α and IL-6 at the comparable level for the HFIP-derived scaffolds (Fig. 9). The expression level in the rest of aqueous-derived scaffolds was significantly lower (Fig. 9).

At the end of 8 weeks, the overall expression levels for all the transcripts evaluated remained low (Fig. 9). The IFN-γ was the only gene that showed an upregulated expression level across all but one experimental group at the end of 8 weeks compared to 2 weeks (Fig. 9). The relative expression level for TNF-α mRNAs in aqueous-derived scaffolds prepared from 10% silk fibroin solution significantly dropped at the end of 8 weeks in comparison to 2 weeks and became comparable to the other aqueous-derived scaffolds (Fig. 9). However, no other trend was clearly demonstrated in any other experimental groups for TNF-α mRNA (Fig. 9). No clear trend was found for the expression of IL-6 mRNAs (Fig. 9). The relative expression levels for IL-4 and IL-13 mRNAs remained too low to make any comparison meaningful (Fig. 9).

3.2.5 Long term Immune response (6 to 12 months)—Throughout the one year implantation, the HFIP and water-based scaffolds were well tolerated by the host animals and no abnormal conditions were observed. While 11 out of 12 aqueous-derived scaffolds prepared from 6% silk fibroin solution were completely degraded by the host animals after 6 months and 12 months as described previously in section 3.2.3, those prepared from 10% silk fibroin solution were left with a few separate pieces with signs of significant degradation (Table 2 and Fig. 10 A, C and D). After 6 months *in vivo*, very few macrophages were present around the remaining small pieces of aqueous-derived scaffolds (Fig. 10 A as an example), while HFIP-derived scaffolds were still surrounded by macrophages (Fig. 10 B as an example).

The critical role macrophages played in the degradation of HFIP-derived scaffolds became quite clear at the end of one year. In general, HFIP-derived scaffolds prepared from higher concentration silk fibroin solutions, especially those with small pore sizes, granted less access to macrophage invasion and thus showed more resistance to macrophage-mediated degradation (Fig. 11). For example, at the end of one year, HFIP-derived scaffolds prepared from 17% silk fibroin solution still had pores not reached by macrophages, which was not observed in scaffolds prepared from lower concentration silk fibroin solutions (Fig. 11). For

HFIP-derived scaffolds prepared from 17% silk fibroin solution with small pore sizes (100 to 200 μm), the peripheral regions that were accessible to macrophages showed signs of degradation and loss of structural integrity, while the scaffolds remained largely intact inside due to the absence of macrophages (Fig. 11).

At the end of 6 months, the overall expression levels for all the genes evaluated decreased compared to 8 weeks, most evidently for IL-6 and IFN-γ (Fig. 9). As mentioned above, the relative expression level for IFN-γ mRNA increased at the end of 8 weeks compared to 2 weeks (Fig. 9). At the end of 6 months, the level for IFN-γ mRNA dropped back to a very low level comparable to 2 weeks (Fig. 9). At the end of 6 months the relative expression levels for IL-4 and IL-13 mRNAs remained too low to make any comparison meaningful (Fig. 9). At the end of one year, the overall expression levels for all the genes evaluated decreased further and became undetectable in many cases (Fig. 9). The relative expression levels were too low to make any comparison or trend meaningful (Fig. 9). After 6 months, the transcripts were not detected in the skin controls (Fig. 9).

4. Discussion

Successful drug delivery and tissue engineering strategies in most cases require three-dimensional scaffolds with varying but controllable structural, morphological and degradation features matched to the targeted clinical application. The interplay of factors such as pore size, concentration of polymer used in processing, structural stability, tissue ingrowth, and degradation are keys to the understanding of the *in vivo* behavior of three-dimensional porous scaffolds. This understanding forms the basis for determining optimal utility of scaffolds to match specific needs in tissue regeneration. Recent advances have greatly expanded the preparation options and processing windows for three-dimensional silk fibroin porous scaffolds as well as their potential for a wide variety of medical applications [15, 22–42]. In the present study, we systematically investigated the *in vivo* response to three-dimensional silk fibroin porous scaffolds with varying pore sizes, silk fibroin solution concentrations, and processing methods (aqueous vs. HFIP).

The results of the first stage (Stage I) of this study, in which aqueous- and HFIP-derived scaffolds with the same pore size distribution (500 to 600 μm) and original silk fibroin concentration (6%) were implanted intramuscularly in nude and Lewis rats for 8 weeks, offered initial insight into how the immune system responds to and then affects the *in vivo* behavior of these scaffolds. Overall, the scaffolds were well tolerated by the host animals and no abnormal conditions were observed during the 8 weeks of implantation. The impact of the immune system on the scaffolds was obvious for the aqueous-derived scaffolds, which significantly shrank in size due to the loss of structural integrity from significant degradation in Lewis rats compared to nude rats. The outcome was not as obvious in the HFIP-derived scaffolds, which showed no significant difference in degradability between the two types of rats during the relatively short implantation time. All aqueous-derived scaffolds lost their structural integrity and were completely infiltrated at the end of 8 weeks. In contrast, all HFIP-derived scaffolds held their structural integrity to some extent, especially in the center of the scaffolds where tissue ingrowth was limited. In Lewis rats, aqueous-derived scaffolds showed clear signs of macrophage-mediated degradation at the end of 8 weeks, which was not common in HFIP-derived scaffolds. These observations demonstrate that both processing methods (aqueous vs. HFIP) and host immune system responses have significant impact on the *in vivo* behavior of three-dimensional silk fibroin porous scaffolds. The effect of cytokines, enzymes, and other factors that are not related to the immune system on the degradation of the scaffolds was rather moderate when compared to immune system-related cellular components including macrophages.

These observations merited the longer Stage II study in hosts with an intact immune system, such as Lewis rats, to better understand the interplay of scaffold processing factors and degradation response. In Stage II, we systematically examined how scaffolds with varying original silk fibroin concentrations and pore sizes impact degradation processes when implanted subcutaneously in Lewis rats. Subcutaneous implantation has the advantage of allowing a large number of samples to be easily placed when compared to intramuscular implantation. The intramuscular sites used in Stage I optimized the likelihood of detecting an immune response and fostering degradation, since blood supply and cellular access is greater at an intramuscular location than a subcutaneous location. The subsequent use of subcutaneous placement in Stage II therefore represented a greater challenge to degradability for all implants, representing a 'worse case scenario'.

In Stage II both short term (2 and 8 weeks) and the long term (6 and 12 months) implants were assessed. At the end of 8 weeks, the morphology of subcutaneously implanted scaffolds in Stage II was similar to that of those intramuscularly implanted scaffolds in Stage I. Tissue ingrowth was more advanced in the aqueous-derived scaffolds than the HFIP-derived scaffolds during the initial period of implantation. HFIP-derived scaffolds held their structural integrity longer than the aqueous-derived scaffolds. Since our prior studies did not indicate a significant different in overall crystallinity between the aqueous vs. solvent processes, we speculate that the sizes of the beta sheet crystals present, or the nature of the crystalline structures present, may be different, as silk is known to exhibit at least three polymorphs.

For the aqueous-derived scaffolds, the concentration of the original silk fibroin solution played a more significant role than pore size with regard to the ability to hold structural integrity *in vivo*. For example, with the same pore size (850 to 1000 μm), scaffolds prepared from 10% silk fibroin solution held their structural integrity for at least 8 weeks, while those prepared from 6% solution did not. It is interesting to note that this effect was also observed in vitro when enzymatic digestion of porous silk scaffolds was characterized [24]. For the HFIP-derived scaffolds, the original silk fibroin concentration and pore size were equally influential to their *in vivo* behavior. The combination of high original silk fibroin concentration and small pore size best reduced tissue ingrowth, and were in some cases still incompletely infiltrated even after 1 year *in vivo*. As a result, this combination significantly slowed down the degradation of the scaffolds. At the end of 1 year, while remains of all HFIP-derived scaffolds were present, those prepared from 17% silk fibroin solution with 100 to 200 μm pore size were the least degraded. In contrast, no aqueous-derived scaffolds held their structural integrity for longer than 6 months, further indicating the fundamental differences between these two types of scaffold. These results can be used to guide the design and selection of three-dimensional silk fibroin scaffolds for specific applications. For example, shorter term drug release systems can be best matched by the aqueous scaffold systems for their fast degradation profile while long-term bone regeneration needs can be best met by the HFIP systems for their slow degradation.

Throughout the study, the scaffolds were tolerated well by the host animals and no abnormal conditions were observed. Histologically the scaffolds did not appear to be heavily enveloped by fibrous tissues in most cases. Macrophages quickly invaded the implantation site and were readily visible around the scaffolds at 2 weeks. At the end of 8 weeks, giant cells were present adjacent to the scaffold. During the initial period of implantation, no clear difference in the number and pattern of macrophages between the aqueous- and the HFIP-derived scaffolds was observed under the microscope. Clear signs of material degradation were evident in the aqueous-derived scaffolds earlier than in the HFIP-derived scaffolds. As a result, the HFIP-derived scaffolds lasted longer *in vivo* than the aqueous-derived scaffolds. By 6 months, most (11 out of 12) aqueous-derived scaffolds prepared from 6% silk fibroin

solution were completely degraded, while all HFIP-derived scaffolds were still present with varying degrees of degradation. At the end of one year, 15 out of 18 aqueous-derived scaffolds were completely degraded and only traces or very few small remaining pieces were found in the other 3 scaffolds. In contrast, remains of all HFIP-derived scaffolds were detected, although most scaffolds had been significantly degraded.

These differences are related to the structural, morphological, and surface characteristics of aqueous- vs. HFIP-derived scaffolds. Previous studies have shown that the aqueous-derived scaffolds provide better interconnected pores and a rougher surface than the HFIP-derived scaffolds, that can improve initial cell attachment and tissue ingrowth [15, 24]. These features contribute to the different outcomes observed with the *in vivo* assessments. During the formation of these scaffolds, silk fibroin used in the process generally undergoes a structural transition from random coil to β-sheet crystals [24, 25]. While total content of beta sheet crystals is not significantly different (between 45–50%) between the water- and HFIP-derived scaffolds, the distribution and sizes of the crystals may vary, contributing to the different rates of degradation, along with the morphological features mentioned above [43]. These differences result in the different behavior of the two types of scaffolds *in vivo*. Further, as mentioned earlier, the presence of different polymorphs of silk, may also contribute to the different functional outcomes in terms of degradation rates.

In general, compared to HFIP-derived scaffolds, the degradation of aqueous-derived scaffolds appeared to be much more homogeneous because of the widespread cellular invasion through out the scaffold. On a macro-scale, the degradation of HFIP scaffolds seems to start from the peripheral regions and slowly progresses towards the center. This resembles the degradation of silk fibers, which starts from the surface via proteolytic activity [44]. However, the present study does not provide sufficient enough evidence at the molecular level to show whether these observations mean that the aqueous-derived scaffolds follow a bulk degradation mechanism while HFIP-derived scaffolds follow a surface degradation mechanism.

At the mRNA level, the expression of inflammation-related genes generally remained low and local throughout the study. Two out the five genes evaluated, IL-4 and IL-13, were barely detectable or not detectable at all. The expression of TNF-α, IL-6, and IFN-γ was weakly detectable during the early period of implantation but dropped to insignificant levels or became undetectable for most experimental groups by 6 months. The only gene, whose expression showed a noticeable increase from 2 weeks to 8 weeks, although still at a very low level, was IFN-γ, reflecting its nature as a late-responding inflammation-related gene. At the end of one year, none of the genes evaluated in the present study were expressed at a meaningful level. These results showed that the host immune response to the implanted scaffolds is low or mild and local, consistent with previous studies [22, 29, 33].

There have been a number of biodegradable polymers widely explored as biomaterials and scaffold systems for tissue engineering applications. Collagen, the most abundant and omnipresent structural protein in the body, has been used for many types of biomedical applications, with degradation affected by the cross-linking and ranging from 1 to 4 weeks or longer *in vivo* [45]. The synthetic biodegradable polymer poly(lactic-*co*-glycolic acid) (PLGA) is also widely used. Degradation time for PLGA (85:15) was about 26 weeks, and for PLGA (50:50) about 6–8 weeks in vitro [46]), with similar results reported *in vivo* [47, 48]. Polycaprolactone (PCL) is another FDA-approved biodegradable polymer that can remain in the body for more than two years [49]. The results reported in the present study suggest that silk fibroin systems offer a range of degradation that encompasses most of the other degradable polymeric scaffolds in common use today. Furthermore, the silk fibroin systems offer many advantages such as avoidance of the need for post processing cross-

linking due to the robust beta sheet formation, compatibility with autoclaving for sterilization without loss of structural integrity, and ability to be processed in all water systems to allow further functionalization with cell signaling factors, DNA, RNA or other components.

5. Conclusions

The present study systematically investigated the interplay of many factors such as processing condition, pore size, silk fibroin concentration, and host immune system elements during *in vivo* degradation of three-dimensional silk fibroin scaffolds. The results showed that the *in vivo* behavior of the silk fibroin scaffolds depended on the original preparation method and structural characteristics. With the demonstrated flexibility and versatility of silk fibroin scaffold processing, these results indicate that the *in vivo* behavior of the silk fibroin scaffolds can be predicted and thus controlled to match the diverse needs for the engineering and repair of various tissues with specific functional requirements, repair characteristics, and repair rates. The information obtained in the present study is important for the further investigation of silk fibroin scaffolds, which have shown potential in a wide variety of medical applications [15, 22, 26–42]. Furthermore, the insights gained can serve as a general guide for scaffold designs in tissue engineering.

Acknowledgments

We thank the NIH Tissue Engineering Resource Center (P41 EB002520) and the NIH NIBIB (R01 EB003210) for support for the study.

References

1. Kaplan D, Adams WW, Farmer B, Viney C. Silk - Biology, Structure, Properties, and Genetics. Acs Sym Ser. 1994; 544:2–16.
2. Kaplan, DL.; Mello, CM.; Arcidiacono, S.; Fossey, S.; Senecal, K.; Muller, W. Silk. In: McGrath, K.; Kaplan, DL., editors. Protein based materials. Boston: Birkhauser; 1998. p. 103-131.
3. Vollrath F, Knight DP. Liquid crystalline spinning of spider silk. Nature. 2001; 410(6828):541–548. [PubMed: 11279484]
4. Winkler S, Kaplan DL. Molecular biology of spider silk. J Biotechnol. 2000; 74(2):85–93. [PubMed: 11763505]
5. Wong Po Foo C, Kaplan DL. Genetic engineering of fibrous proteins: spider dragline silk and collagen. Adv Drug Deliv Rev. 2002; 54(8):1131–1143. [PubMed: 12384311]
6. Altman GH, Diaz F, Jakuba C, Calabro T, Horan RL, Chen J, et al. Silk-based biomaterials. Biomaterials. 2003; 24(3):401–416. [PubMed: 12423595]
7. Kaplan DL. Fibrous proteins - silk as a model system. Polym Degrad Stabil. 1998; 59(1–3):25–32.
8. Vollrath F. Biology of spider silk. Int J Biol Macromol. 1999; 24(2–3):81–88. [PubMed: 10342751]
9. Rising A, Nimmervoll H, Grip S, Fernandez-Arias A, Storckenfeldt E, Knight DP, et al. Spider silk proteins--mechanical property and gene sequence. Zoolog Sci. 2005; 22(3):273–281. [PubMed: 15795489]
10. Deveikis JP, Manz HJ, Luessenhop AJ, Caputy AJ, Kobrine AI, Schellinger D, et al. A clinical and neuropathologic study of silk suture as an embolic agent for brain arteriovenous malformations. AJNR Am J Neuroradiol. 1994; 15(2):263–271. [PubMed: 8192071]
11. Abi Rached RS, de Toledo BE, Okamoto T, Marcantonio Junior E, Sampaio JE, Orrico SR, et al. Reaction of the human gingival tissue to different suture materials used in periodontal surgery. Braz Dent J. 1992; 2(2):103–113. [PubMed: 1290909]
12. Durdey P, Bucknall TE. Assessment of sutures for use in colonic surgery: an experimental study. J R Soc Med. 1984; 77(6):472–477. [PubMed: 6429330]

13. Salthouse TN, Matlaga BF, Wykoff MH. Comparative tissue response to six suture materials in rabbit cornea, sclera, and ocular muscle. Am J Ophthalmol. 1977; 84(2):224–233. [PubMed: 888893]

14. Salthouse TN. Biologic response to sutures. Otolaryngol Head Neck Surg. 1980; 88(6):658–664. [PubMed: 7010269]

15. Wang Y, Kim HJ, Vunjak-Novakovic G, Kaplan DL. Stem cell-based tissue engineering with silk biomaterials. Biomaterials. 2006; 27(36):6064–6082. [PubMed: 16890988]

16. Minoura N, Aiba S, Higuchi M, Gotoh Y, Tsukada M, Imai Y. Attachment and growth of fibroblast cells on silk fibroin. Biochem Biophys Res Commun. 1995; 208(2):511–516. [PubMed: 7695601]

17. Minoura N, Aiba S, Gotoh Y, Tsukada M, Imai Y. Attachment and growth of cultured fibroblast cells on silk protein matrices. J Biomed Mater Res. 1995; 29(10):1215–1221. [PubMed: 8557723]

18. Gotoh Y, Tsukada M, Minoura N. Effect of the chemical modification of the arginyl residue in Bombyx mori silk fibroin on the attachment and growth of fibroblast cells. J Biomed Mater Res. 1998; 39(3):351–357. [PubMed: 9468042]

19. Inouye K, Kurokawa M, Nishikawa S, Tsukada M. Use of Bombyx mori silk fibroin as a substratum for cultivation of animal cells. J Biochem Biophys Methods. 1998; 37(3):159–164. [PubMed: 9870190]

20. Santin M, Motta A, Freddi G, Cannas M. In vitro evaluation of the inflammatory potential of the silk fibroin. J Biomed Mater Res. 1999; 46(3):382–389. [PubMed: 10397996]

21. Sugihara A, Sugiura K, Morita H, Ninagawa T, Tubouchi K, Tobe R, et al. Promotive effects of a silk film on epidermal recovery from full-thickness skin wounds. Proc Soc Exp Biol Med. 2000; 225(1):58–64. [PubMed: 10998199]

22. Meinel L, Hofmann S, Karageorgiou V, Kirker-Head C, McCool J, Gronowicz G, et al. The inflammatory responses to silk films in vitro and in vivo. Biomaterials. 2005; 26(2):147–155. [PubMed: 15207461]

23. Kim HJ, Kim HS, Matsumoto A, Chin IJ, Jin HJ, Kaplan DL. Processing windows for forming silk fibroin biomaterials into a 3D porous matrix. Aust J Chem. 2005; 58(10):716–720.

24. Kim UJ, Park J, Kim HJ, Wada M, Kaplan DL. Three-dimensional aqueous-derived biomaterial scaffolds from silk fibroin. Biomaterials. 2005; 26(15):2775–2785. [PubMed: 15585282]

25. Nazarov R, Jin HJ, Kaplan DL. Porous 3-D scaffolds from regenerated silk fibroin. Biomacromolecules. 2004; 5(3):718–726. [PubMed: 15132652]

26. Kim HJ, Kim UJ, Vunjak-Novakovic G, Min BH, Kaplan DL. Influence of macroporous protein scaffolds on bone tissue engineering from bone marrow stem cells. Biomaterials. 2005; 26(21): 4442–4452. [PubMed: 15701373]

27. Meinel L, Karageorgiou V, Fajardo R, Snyder B, Shinde-Patil V, Zichner L, et al. Bone tissue engineering using human mesenchymal stem cells: effects of scaffold material and medium flow. Ann Biomed Eng. 2004; 32(1):112–122. [PubMed: 14964727]

28. Meinel L, Karageorgiou V, Hofmann S, Fajardo R, Snyder B, Li C, et al. Engineering bone-like tissue in vitro using human bone marrow stem cells and silk scaffolds. J Biomed Mater Res A. 2004; 71(1):25–34. [PubMed: 15316936]

29. Meinel L, Fajardo R, Hofmann S, Langer R, Chen J, Snyder B, et al. Silk implants for the healing of critical size bone defects. Bone. 2005; 37(5):688–698. [PubMed: 16140599]

30. Meinel L, Hofmann S, Karageorgiou V, Zichner L, Langer R, Kaplan D, et al. Engineering cartilage-like tissue using human mesenchymal stem cells and silk protein scaffolds. Biotechnol Bioeng. 2004; 88(3):379–391. [PubMed: 15486944]

31. Wang YZ, Kim UJ, Blasioli DJ, Kim HJ, Kaplan DL. In vitro cartilage tissue engineering with 3D porous aqueous-derived silk scaffolds and mesenchymal stem cells. Biomaterials. 2005; 26(34): 7082–7094. [PubMed: 15985292]

32. Wang YZ, Blasioli DJ, Kim HJ, Kim HS, Kaplan DL. Cartilage Tissue Engineering with Silk Scaffolds and Human Articular Chondrocytes. Biomaterials. 2006 In press.

33. Kirker-Head C, Karageorgiou V, Hofmann S, Fajardo R, Betz O, Merkle HP, et al. BMP-silk composite matrices heal critically sized femoral defects. Bone. 2007; 41(2):247–255. [PubMed: 17553763]

34. Hofmann S, Hagenmuller H, Koch AM, Muller R, Vunjak-Novakovic G, Kaplan DL, et al. Control of in vitro tissue-engineered bone-like structures using human mesenchymal stem cells and porous silk scaffolds. Biomaterials. 2007; 28(6):1152–1162. [PubMed: 17092555]
35. Hagenmuller H, Hofmann S, Kohler T, Merkle HP, Kaplan DL, Vunjak-Novakovic G, et al. Non-Invasive Time-Lapsed Monitoring and Quantification of Engineered Bone-Like Tissue. Ann Biomed Eng. 2007
36. Uebersax L, Hagenmuller H, Hofmann S, Gruenblatt E, Muller R, Vunjak-Novakovic G, et al. Effect of scaffold design on bone morphology in vitro. Tissue Eng. 2006; 12(12):3417–3429. [PubMed: 17518678]
37. Meinel L, Hofmann S, Betz O, Fajardo R, Merkle HP, Langer R, et al. Osteogenesis by human mesenchymal stem cells cultured on silk biomaterials: comparison of adenovirus mediated gene transfer and protein delivery of BMP-2. Biomaterials. 2006; 27(28):4993–5002. [PubMed: 16765437]
38. Meinel L, Betz O, Fajardo R, Hofmann S, Nazarian A, Cory E, et al. Silk based biomaterials to heal critical sized femur defects. Bone. 2006; 39(4):922-–931. [PubMed: 16757219]
39. Karageorgiou V, Tomkins M, Fajardo R, Meinel L, Snyder B, Wade K, et al. Porous silk fibroin 3-D scaffolds for delivery of bone morphogenetic protein-2 in vitro and in vivo. J Biomed Mater Res A. 2006; 78(2):324–334. [PubMed: 16637042]
40. Hofmann S, Knecht S, Langer R, Kaplan DL, Vunjak-Novakovic G, Merkle HP, et al. Cartilage-like tissue engineering using silk scaffolds and mesenchymal stem cells. Tissue Eng. 2006; 12(10): 2729–2738. [PubMed: 17518642]
41. Wang Y, Kim UJ, Blasioli DJ, Kim HJ, Kaplan DL. In vitro cartilage tissue engineering with 3D porous aqueous-derived silk scaffolds and mesenchymal stem cells. Biomaterials. 2005; 26(34): 7082–7094. [PubMed: 15985292]
42. Vunjak-Novakovic G, Meinel L, Altman G, Kaplan D. Bioreactor cultivation of osteochondral grafts. Orthod Craniofac Res. 2005; 8(3):209–218. [PubMed: 16022723]
43. Jin HJ, J P, Karageorgiou V, Kim UJ, Valluzzi R, Cebe P, et al. Water-Stable Silk Films with Reduced beta-Sheet Content. Advanced Functional Materials. 2005; 15(8):1241–1247.
44. Horan RL, Antle K, Collette AL, Wang Y, Huang J, Moreau JE, et al. In vitro degradation of silk fibroin. Biomaterials. 2005; 26(17):3385–3393. [PubMed: 15621227]
45. Ueda H, Hong L, Yamamoto M, Shigeno K, Inoue M, Toba T, et al. Use of collagen sponge incorporating transforming growth factor-beta 1 to promote bone repair in skull defects in rabbits. Biomaterials. 2002; 23(4):1003–1010. [PubMed: 11791902]
46. Ramchandani M, Pankaskie M, Robinson D. The influence of manufacturing procedure on the degradation of poly(lactide-co-glycolide) 85:15 and 50:50 implants. Journal of Controlled Release. 1997; 43(2–3):161–173.
47. Kister G, Cassanas G, Vert M. Structure and morphology of solid lactide-glycolide copolymers from C-13 nmr, infra-red and Raman spectroscopy. Polymer. 1998; 39(15):3335–3340.
48. Liao S, Watari F, Zhu Y, Uo M, Akasaka T, Wang W, et al. The degradation of the three layered nano-carbonated hydroxyapatite/collagen/PLGA composite membrane in vitro. Dent Mater. 2007; 23(9):1120–1128. [PubMed: 17095082]
49. Sun H, Mei L, Song C, Cui X, Wang P. The in vivo degradation, absorption and excretion of PCL-based implant. Biomaterials. 2006; 27(9):1735–1740. [PubMed: 16198413]

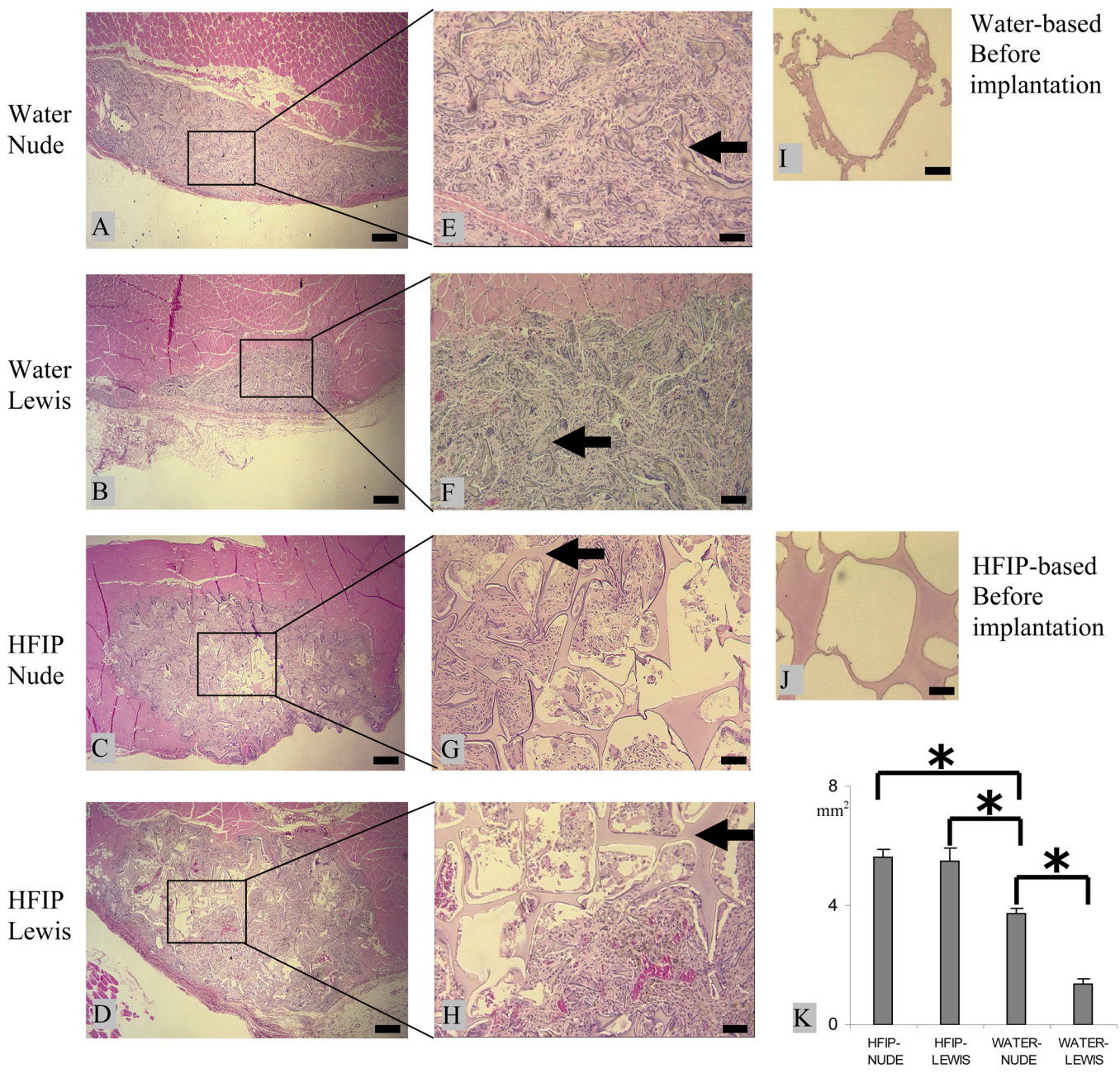

Figure 1.

Intramuscular degradation of aqueous-(A, B, E, and F) and HFIP-(C, D, G, and H) derived silk scaffolds in nude and Lewis rats. Scaffolds were implanted for 8 weeks and stained with H&E. Original structure of the aqueous- and HFIP-derived scaffolds prior to implantation are shown in I and J, respectively. The cross-section area is shown in K. Bars in A–D = 400 μm and in E–J = 100 μm. Solid arrows = remaining scaffolds. ($p<0.05$)

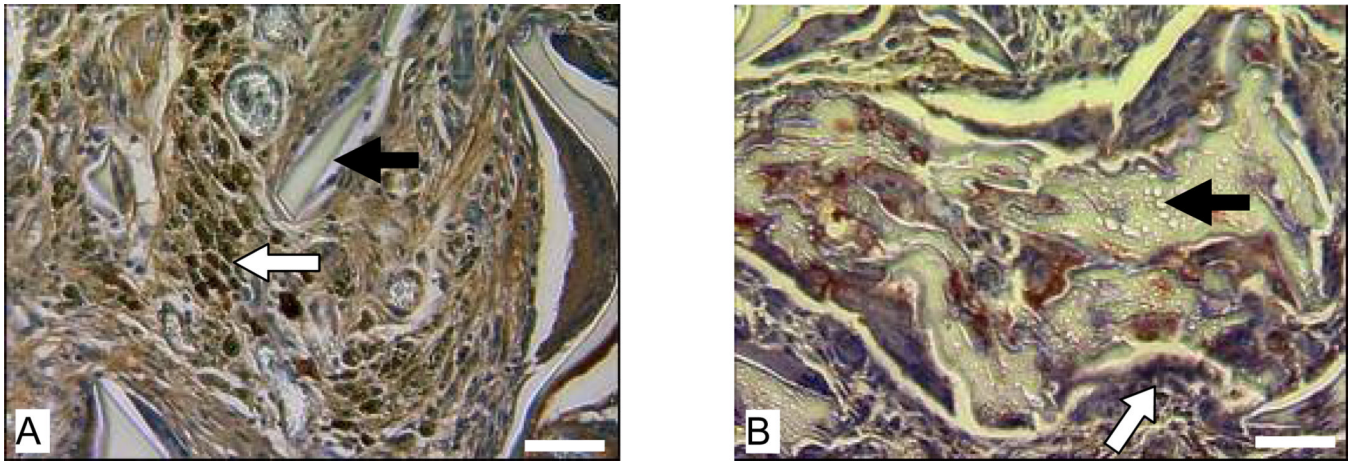

Figure 2.
Host response to intramuscularly implanted silk fibroin scaffolds in Lewis rats at 8 weeks. Images A and B are for HFIP-derived scaffolds and aqueous-derived scaffolds, respectively. Bars = 100 μm. Solid arrows = remaining scaffolds. Blank arrows = ED1 positive cells.

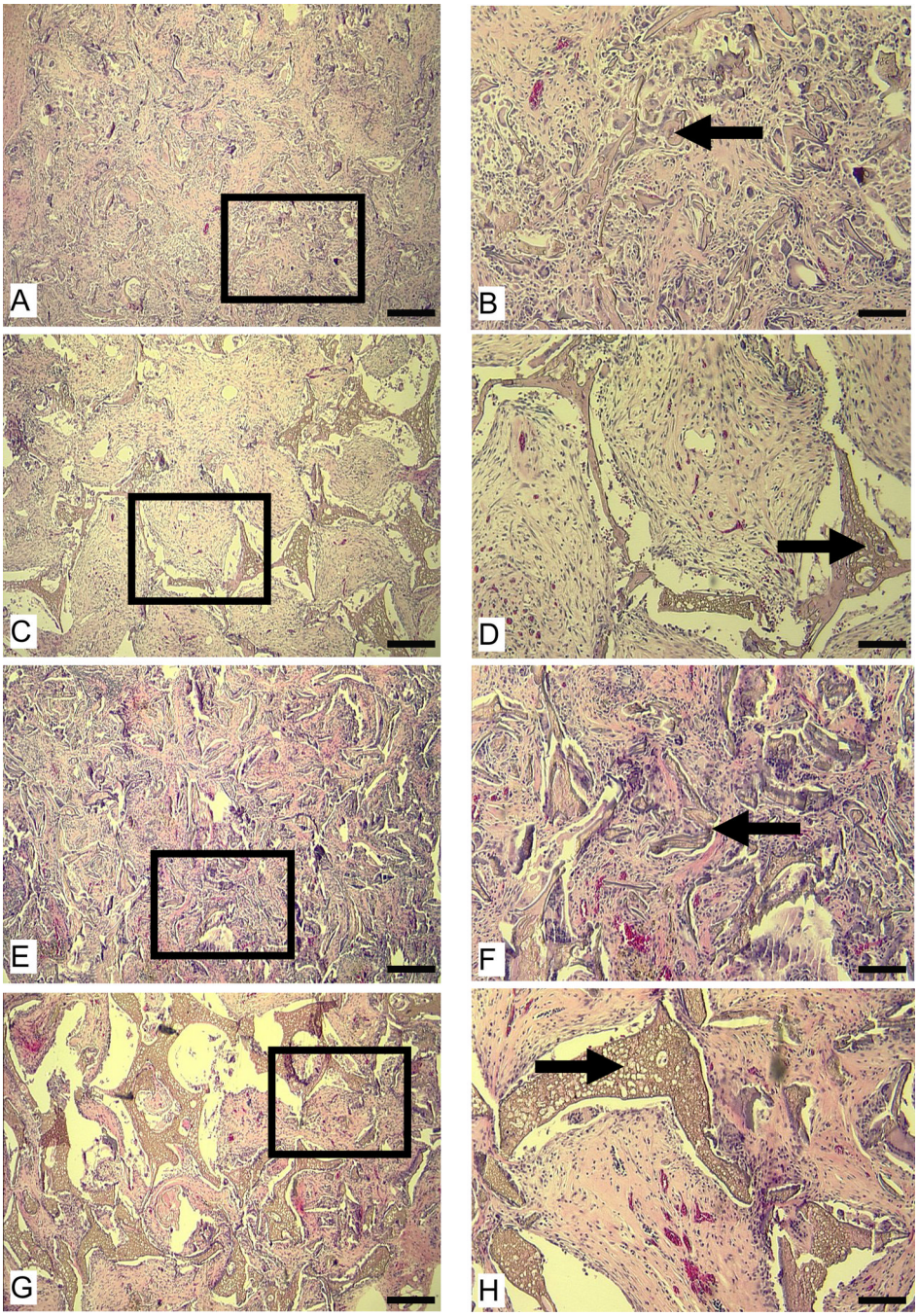

Figure 3.
Morphologies of subcutaneously implanted aqueous-derived silk fibroin scaffolds in Lewis rats at 2 weeks (A–D) and 8 week (E–F). Images A,B, E, and F are for scaffolds with 850–1000 μm pore size prepared from 6% silk fibroin solution. Images C, D, G, and H are for scaffolds with 850–1000 μm pore size prepared from 10% silk fibroin solution. Images B, D, F, H are the enlarged views of the boxed area in Images A, C, E and G, respectively. Bars in images A, C, E, and G = 250 μm and in B, D, F, and H = 100 μm. Solid arrows in images B, D, F, and H = remaining scaffolds.

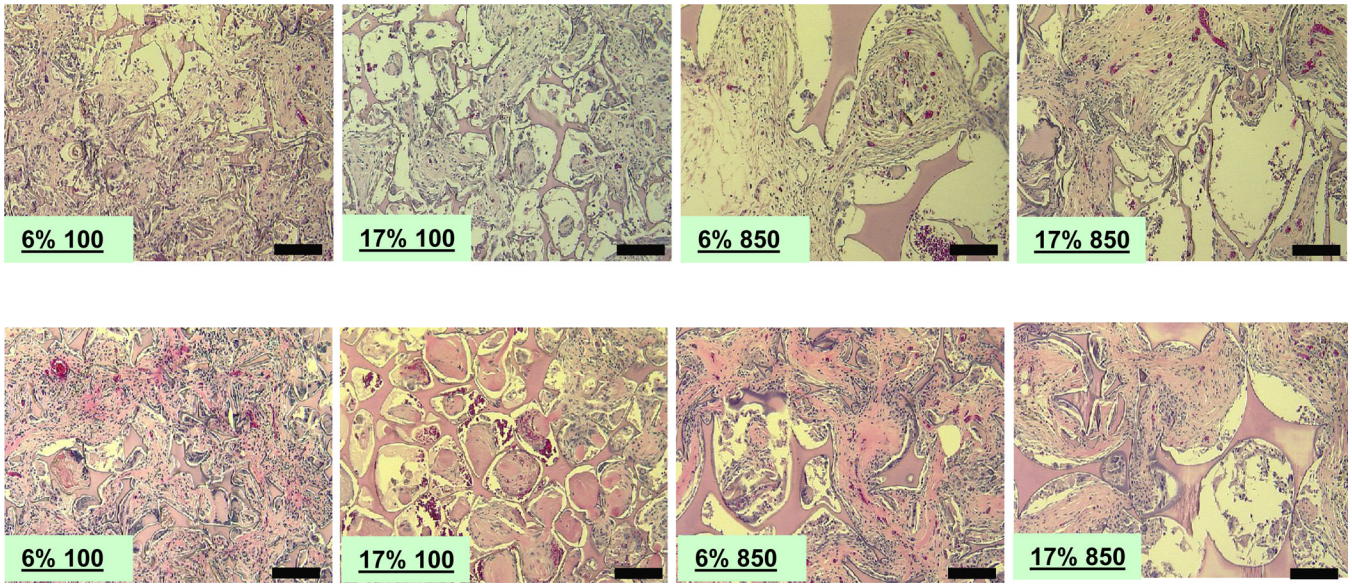

Figure 4.
Morphologies of subcutaneously implanted HFIP-derived silk fibroin scaffolds in Lewis rats at 2 (top row) and 8 weeks (bottom row). Labels in all images describe the original silk fibroin concentration followed by pore size. Due to limitation in space, pore sizes “100” and “850” in the labels refer to 100 – 200 μm and 850 – 1000 μm, respectively. Bars = 100 μm.

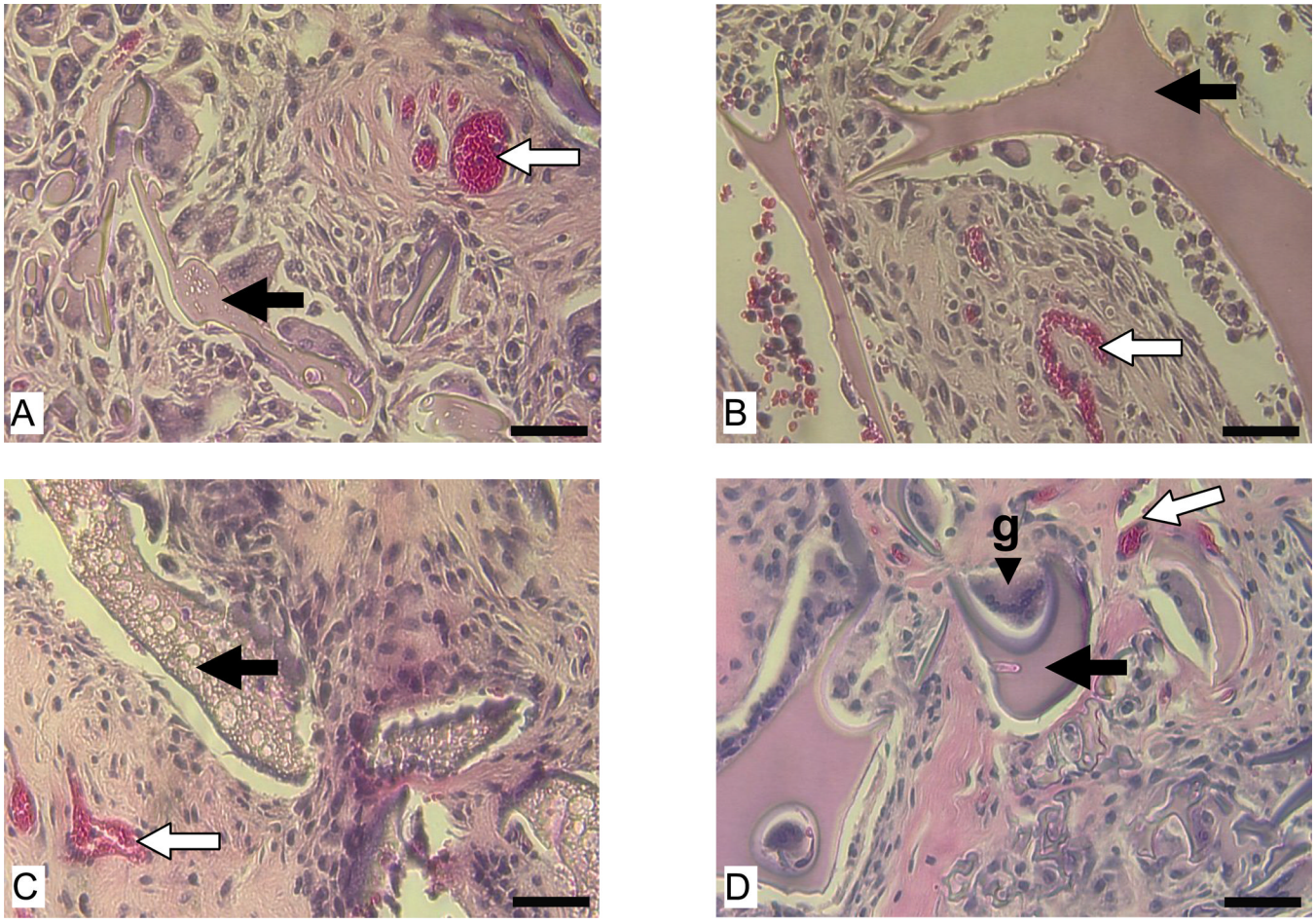

Figure 5.
Vascularization of subcutaneously implanted aqueous and HFIP-derived silk fibroin scaffolds in Lewis rats at 2 and 8 weeks. Images A and C are for aqueous-derived scaffolds at 2 and 8 weeks, respectively. Images B and D are for HFIP-derived scaffolds at 2 and 8 weeks, respectively. Bars= 100 μm. Solid arrows = remaining scaffolds. Blank arrows = signs of vascularization. Abbreviation “g” in image D = giant cell.

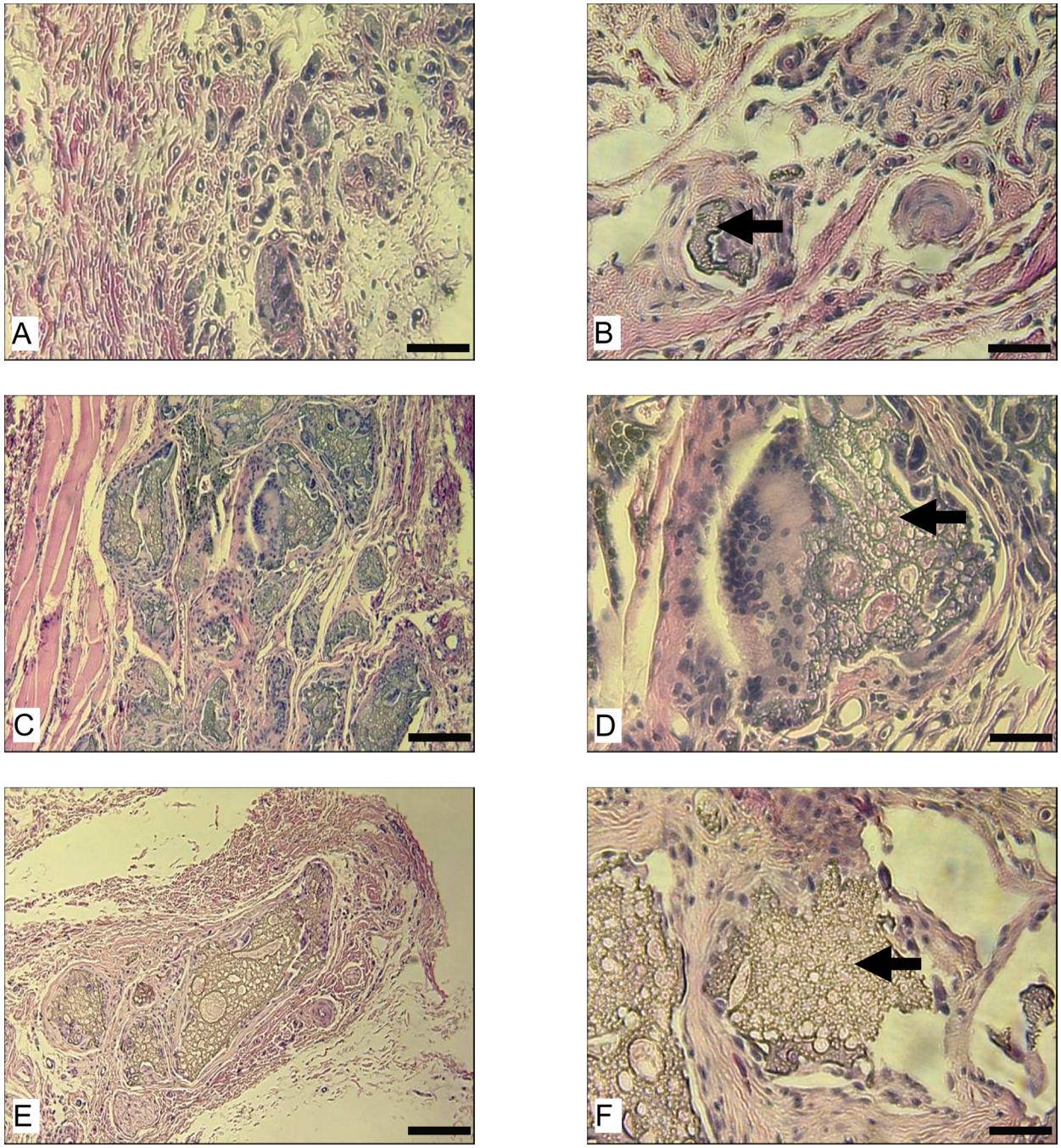

Figure 6.

Morphologies of subcutaneously implanted aqueous-derived silk fibroin scaffolds at 6 and 12 months. Images A and B show the only remaining scaffold prepared from 6% silk fibroin solution with 500 – 600 μm pore size at 6 and 12 months, respectively. Images C and D show the remaining scaffolds prepared from 10% silk fibroin solution with 850 – 1000 μm pore size at 6 months at 10X and 32X, respectively. Images E and F show the remaining scaffolds prepared from 10% silk fibroin solution with 850 – 1000 μm pore size at 12 months at 10X and 32X, respectively. Bars in A, B, D, and F = 100 μm and in C and E = 300 μm. Solid arrows = remaining scaffolds.

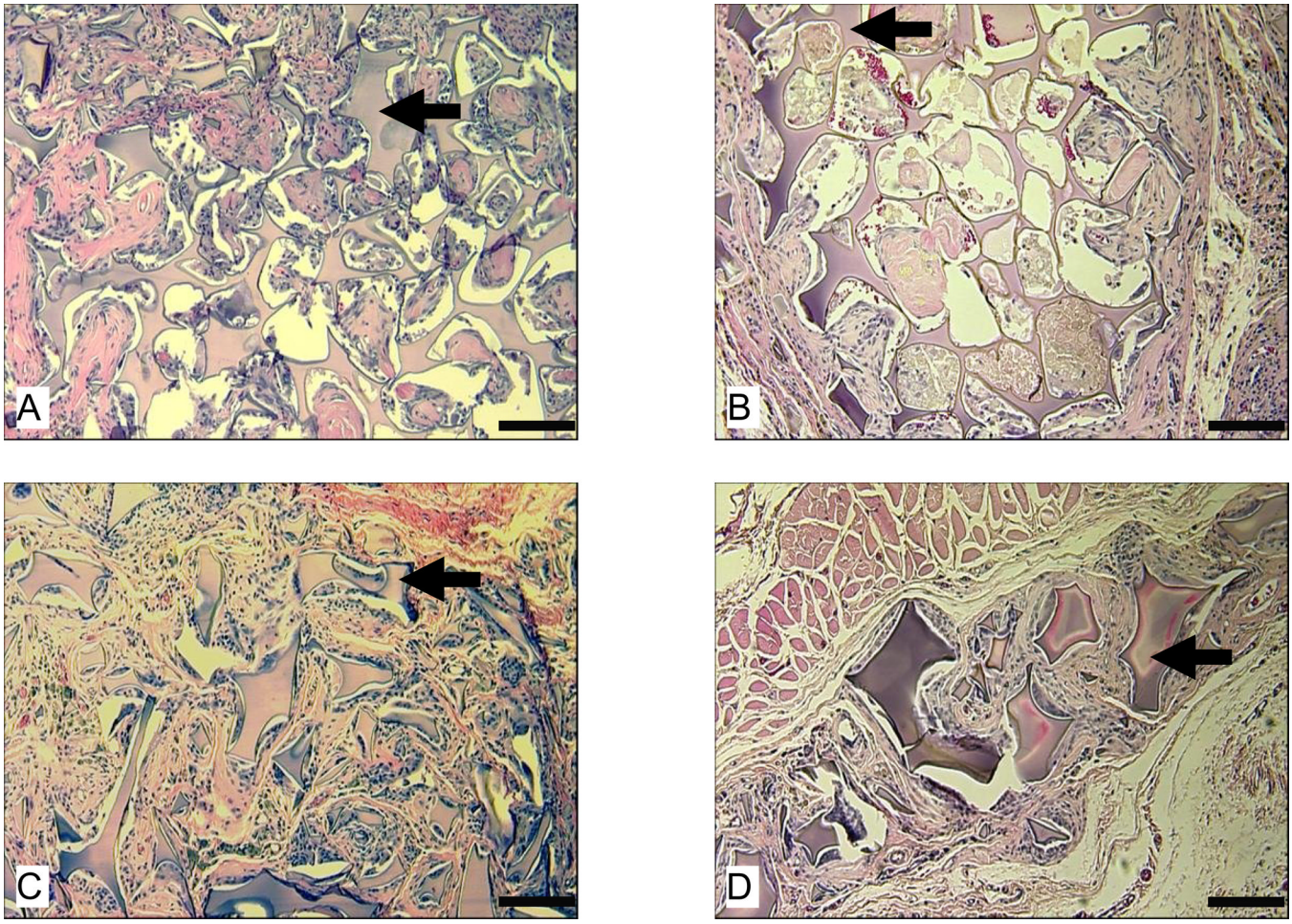

Figure 7.
Morphologies of subcutaneously implanted HFIP-derived silk fibroin scaffolds at 6 and 12 months. Images A and B are for HFIP-derived scaffolds prepared from 17% silk fibroin solution with 100 – 200 μm pore size at 6 months and 12 months, respectively. Images C and D are for HFIP-derived scaffolds prepared from 6% silk fibroin solution with 500 – 600 μm pore size at 6 and 12 months, respectively. Bars = 100 μm. Solid arrows = remaining scaffolds.

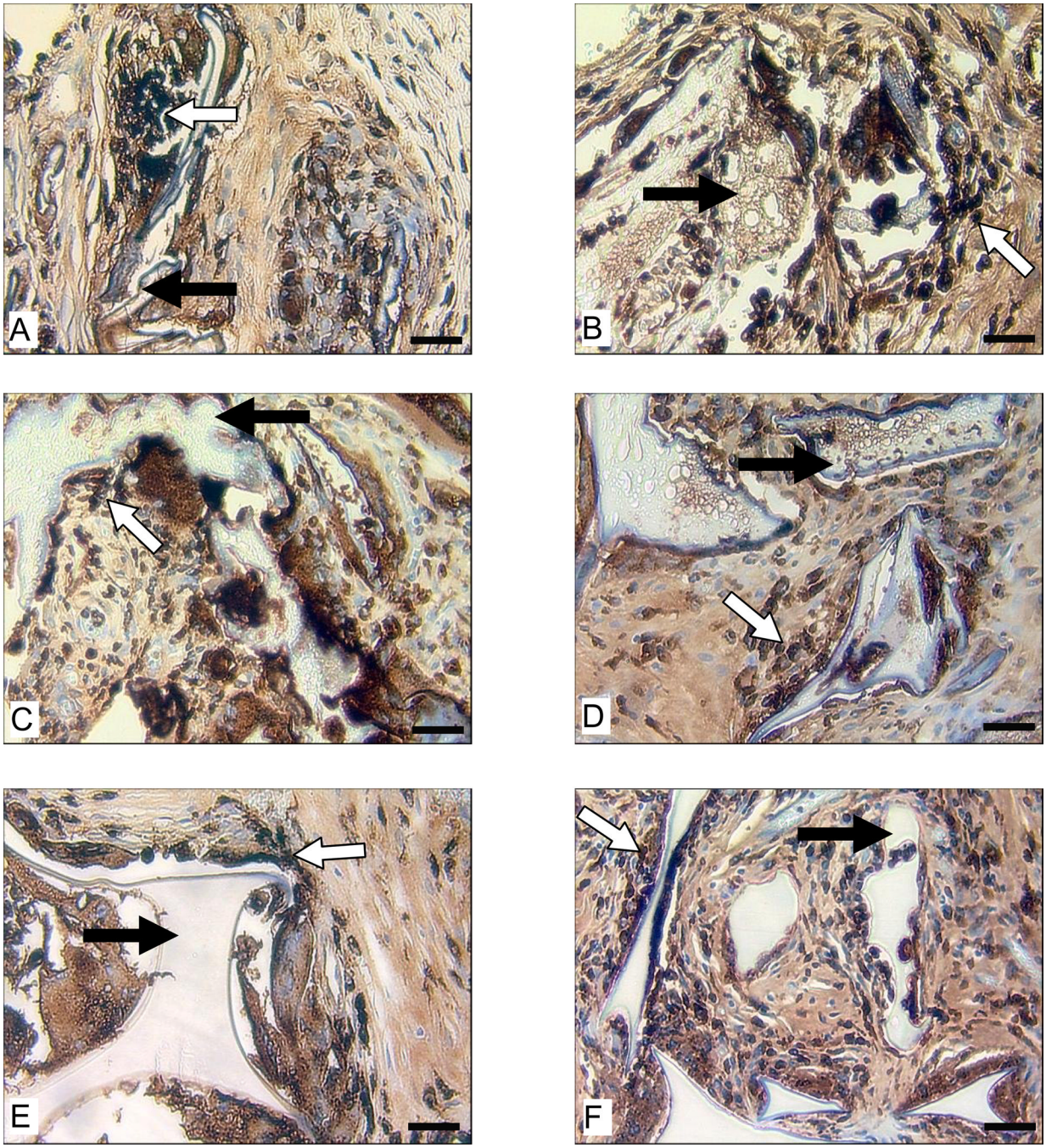

Figure 8.

Macrophage response to subcutaneously implanted scaffolds in Lewis rats. Images A and B are for aqueous-derived silk fibroin scaffolds prepared from 6% and 10% silk fibroin solution at 2 weeks, respectively. Images C and D are for aqueous-derived silk fibroin scaffolds prepared from 6% and 10% silk fibroin solution at 8 weeks, respectively. Images E and F are for HFIP-derived silk fibroin scaffolds prepared from 6% silk fibroin solution at 2 (E) and 8 weeks (F). The pore size of all scaffolds is 850–1000 μm. Bars = 100 μm. Solid arrows = remaining scaffolds. Blank arrows = ED1 positive cells.

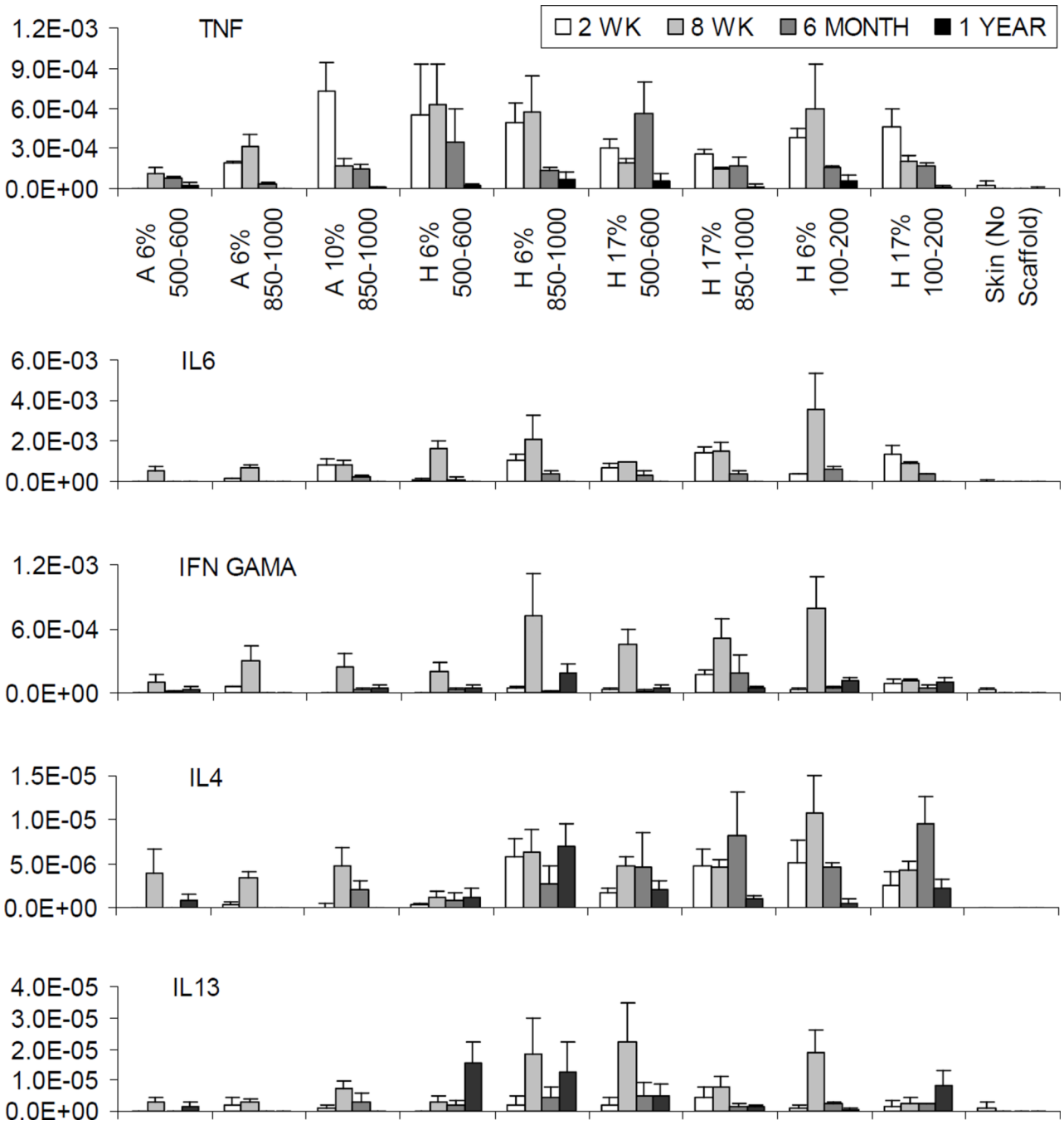

Figure 9.

The relative expression level for TNF-α, IL6, IFN-γ, IL4, and IL13 mRNAs at 2 weeks, 8 weeks, 6 months and 12 months. Labels for X axis: “A” for aqueous and “H” for HFIP. For examples, “A 6% 500–600” represents aqueous-derived scaffolds with 500–600 μm pore size prepared from 6 % silk fibroin solution, while “H 6% 500–600” represents HFIP-derived scaffolds with 500–600 μm pore size prepared from 6 % silk fibroin solution. Y axis = relative expression level normalized to GAPDH. The missing bars in the graphs at varying timepoints indicate relative expression levels were not detectable.

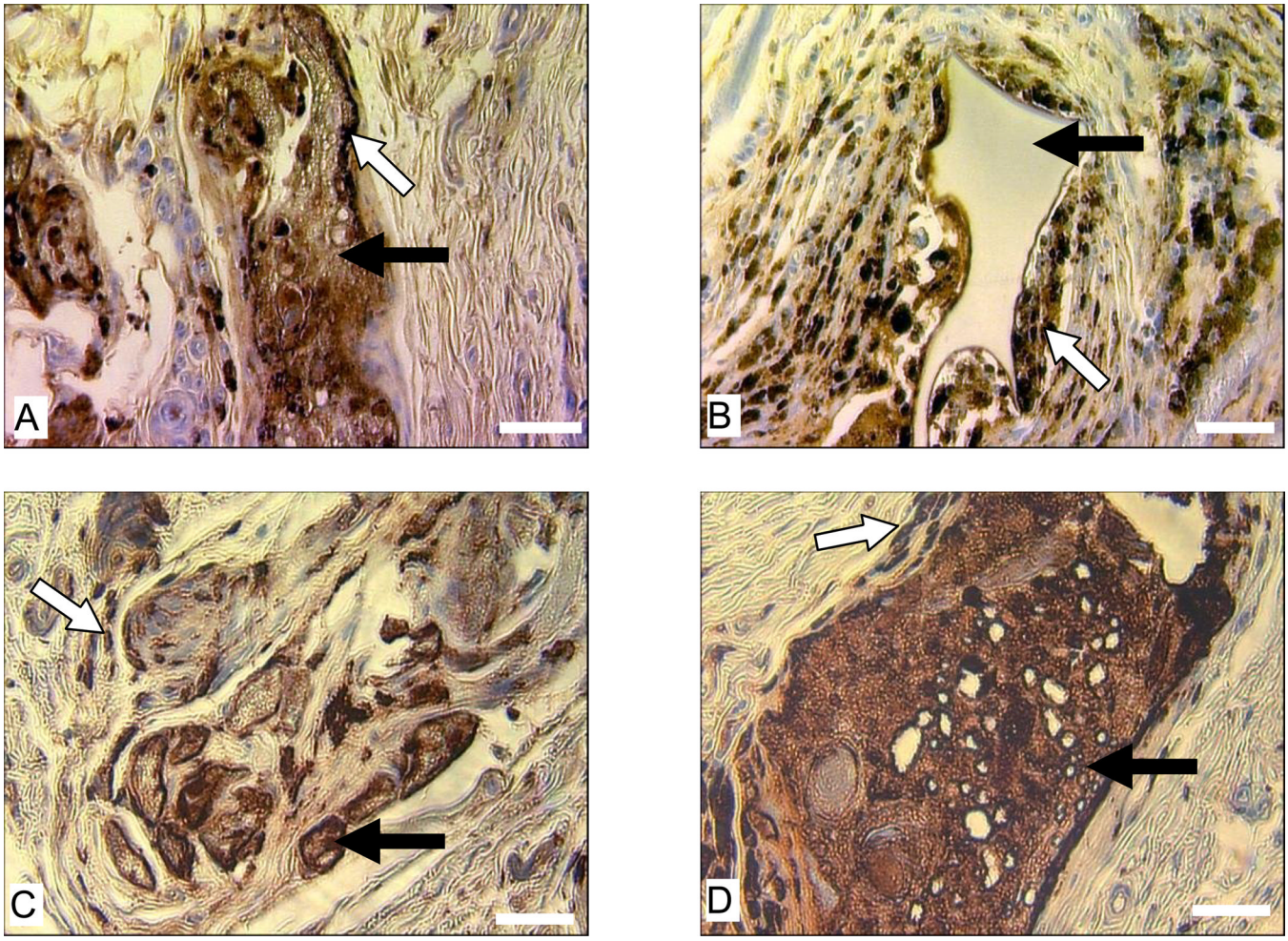

Figure 10.

Morphologies of and macrophage responses to subcutaneously implanted silk fibroin scaffolds in Lewis rats at 6 months (A and B) and 12 months (C and D). Image A is for aqueous-derived scaffold with 850–1000 μm pore size prepared from 10% silk fibroin solution. Image B is for HFIP-derived scaffold with 500–600 μm pore size prepared from 6% silk fibroin solution. Images C and D are for aqueous-derived scaffold with 500–600 μm pore size prepared from 6% silk fibroin solution and with 850–1000 μm pore size prepared from 10% silk fibroin solution, respectively. Bars in A and B = 100 μm and in C and D = 300 μm. Solid arrows = remaining scaffolds. Blank arrows = ED1 positive cells.

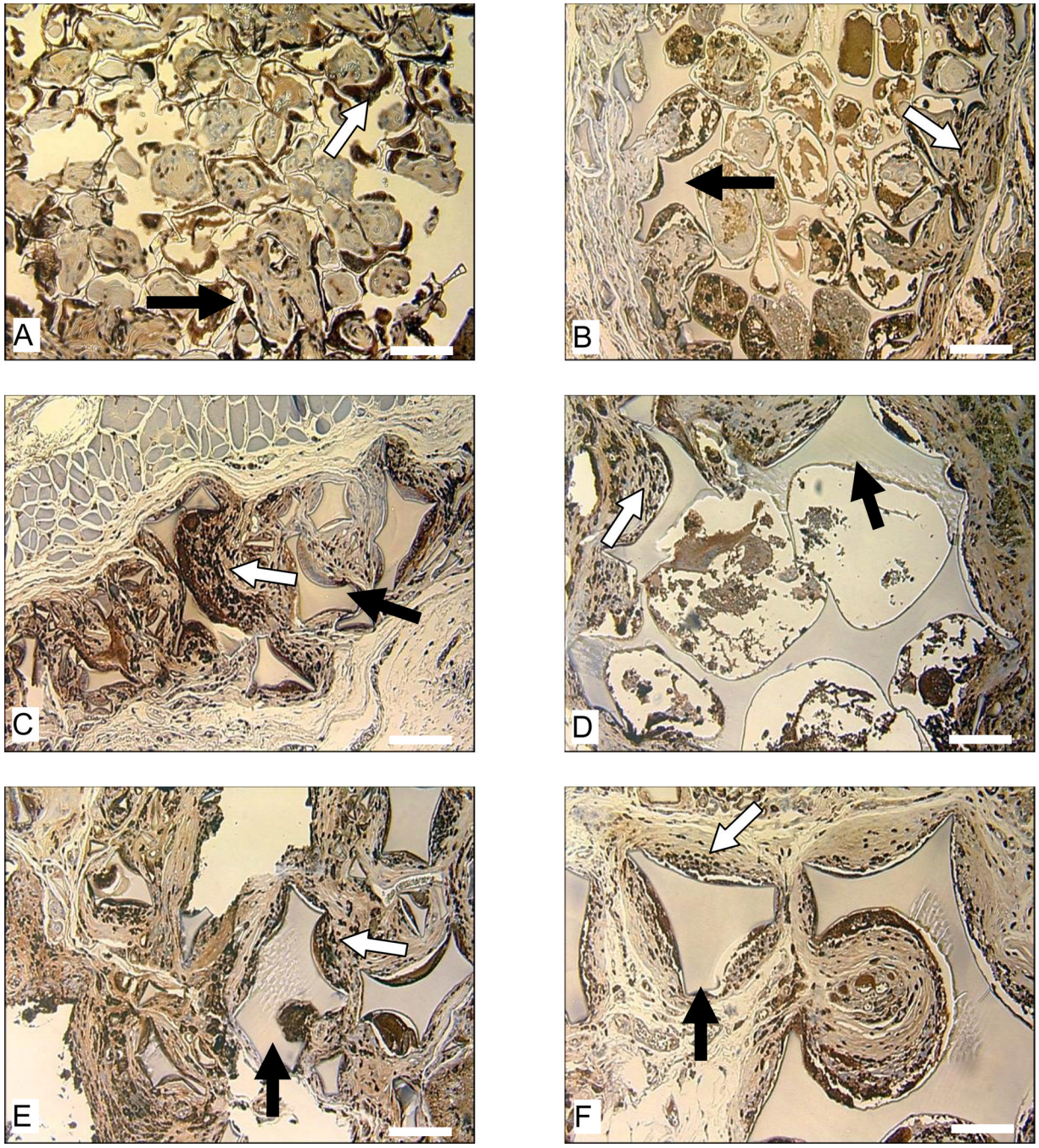

Figure 11.
Macrophage response to subcutaneously implanted HFIP-derived silk fibroin scaffolds in Lewis rats at the end of 12 months. Images A, C, and E are for scaffolds prepared from 6% silk fibroin solution. Images B, D, and F are for scaffolds prepared from 17% silk fibroin solution. Pore size in Images A and B is 100–200 μm, in C and D is 500–600 μm, and in E and F is 850–1000 μm. Bars = 100 μm. Solid arrows = remaining scaffolds. Blank arrows = ED1 positive cells.

Table 1

Experimental design of the study.

Stage I			
Animals and Implantation site	Nude rats and Lewis rats, intramuscular		
Implantation time	8 weeks		
Scaffolds	Aqueous		HFIP
Silk fibroin concentration	6%		6%
Pore size (μm)	500–600		500–600
Total implants (n=4 for histology/immunohistochemistry)	4		4
Stage II			
Animals and Implantation site	Lewis rat, subcutaneous		
Implantation time	2 weeks, 8 weeks, 6 months, and 1 year		
Scaffolds	Aqueous		HFIP
Silk fibroin concentration	6%	10%	6%, 17%
Pore size (μm)	500–600, 850–1000	850–1000	100–200, 500–600, 850–1000
Total implants (n=6, 3 for PCR analysis and 3 for histology/ immunohistochemistry)	96	48	288

Table 2

Statistics of remains found in subcutaneously implanted silk fibroin scaffolds at different time points.

Process	**Water-Derived**			**HFIP-Derived**
Category	**6% (500–600 μm)**	**6% (850–1000 μm)**	**10% (850–1000 μm)**	**6%and 17% (100–200,500–600,and 850–1000 μm)**
Number of samples with residuals / total scaffolds implanted				
At 2 and 8 weeks	6/6	6/6	6/6	36/36 (Residuals found in all samples)
At 6 months	1(trace)/6	0/6	4/6	36/36 (Residuals found in all samples)
At 12 months	1(trace)/6	0/6	2 (very few small pieces) /6	36/36 (Residuals found in all samples)